The Astrophysical Journal, 757:39 (10pp), 2012 September 20 doi:10.1088/0004-637X/757/1/39

XMM-NEWTON VIEW OF SWIFT J1834.9−0846 AND ITS MAGNETAR WIND NEBULA

G. Younes[1,2], C. Kouveliotou[2,3], O. Kargaltsev[4], G. G. Pavlov[5,6], E. Göğüş[7], and S. Wachter[8]
[1] Universities Space Research Association, 6767 Old Madison Pike NW, Suite 450, Huntsville, AL 35806, USA
[2] NSSTC, 320 Sparkman Drive, Huntsville, AL 35805, USA
[3] Astrophysics Office, ZP12, NASA/Marshall Space Flight Center, Huntsville, AL 35812, USA
[4] Department of Astronomy, University of Florida, Bryant Space Science Center, Gainesville, FL 32611, USA
[5] Department of Astronomy and Astrophysics, Pennsylvania State University, 525 Davey Lab, University Park, PA 16802, USA
[6] St.-Petersburg State Polytechnical University, Polytekhnicheskaya ul. 29, 195251 St.-Petersburg, Russia
[7] Faculty of Engineering and Natural Sciences, Sabancı University, Orhanlı-Tuzla, İstanbul 34956, Turkey
[8] Infrared Processing and Analysis Center, California Institute of Technology, Pasadena, CA 91125, USA
Received 2012 April 12; accepted 2012 July 25; published 2012 September 4

ABSTRACT

We report on the analysis of two *XMM-Newton* observations of the recently discovered soft gamma repeater Swift J1834.9−0846, taken in 2005 September and one month after the source went into outburst on 2011 August 7. We performed timing and spectral analyses on the point source as well as on the extended emission. We find that the source period is consistent with an extrapolation of the *Chandra* ephemeris reported earlier and the spectral properties remained constant. The source luminosity decreased to a level of 1.6×10^{34} erg s^{-1} following a decay trend of $\propto t^{-0.5}$. Our spatial analysis of the source environment revealed the presence of two extended emission regions around the source. The first (region A) is a symmetric ring around the point source, starting at 25″ and extending to ∼50″. We argue that region A is a dust scattering halo. The second (region B) has an asymmetrical shape extending between 50″ and 150″, and is detected both in the pre- and post-outburst data. We argue that this region is a possible magnetar wind nebula (MWN). The X-ray efficiency of the MWN with respect to the rotation energy loss is substantially higher than those of rotation-powered pulsars: $\eta_X \equiv L_{\rm MWN,0.5-8\,keV}/\dot{E}_{\rm rot} \approx 0.7$. The higher efficiency points to a different energy source for the MWN of Swift J1834.9−0846, most likely bursting activity of the magnetar, powered by its high magnetic field, $B = 1.4 \times 10^{14}$ G.

Key words: stars: neutron – X-rays: individual (Swift J1834.9−0846) – X-rays: ISM

1. INTRODUCTION

Soft gamma repeaters (SGRs) and anomalous X-ray pulsars (AXPs) are two empirical classes of objects widely accepted to comprise the magnetar population, i.e., isolated neutron stars with ultra-strong magnetic fields ($B \gtrsim 10^{14}$–10^{15} G). Their existence was predicted theoretically in 1992 (Duncan & Thompson 1992; Paczynski 1992), but was only confirmed in 1998 with *RXTE* observations (Kouveliotou et al. 1998, 1999; for detailed magnetar reviews please refer to Woods & Thompson 2006; Mereghetti 2008). SGRs and AXPs share many characteristics such as long spin periods (2–12 s) and large spin-down rates that imply very high surface dipole magnetic fields of 10^{14}–10^{15} G. They are all persistent X-ray emitters with luminosities significantly larger than those expected from rotational energy losses; instead the magnetar X-ray emission is attributed to the decay of their powerful magnetic fields and sub-surface heating (Thompson & Duncan 1996). Magnetars enter active episodes during which they emit short (0.1 s) bursts of hard X-/soft γ-rays with luminosities ranging from 10^{37} to 10^{41} erg s^{-1}; very rarely, they emit giant flares (GFs) that last several minutes with luminosities $\gtrsim 10^{46}$ erg s^{-1}. The typical magnetar bursts are attributed to neutron star crust quakes caused by the evolving magnetic field under its surface (Thompson & Duncan 1995).

An interesting question in the magnetar field is their evolutionary link, if any, to their less magnetically powerful counterparts, rotation-powered pulsars (RPPs). The latter sources are known to produce particle outflows, often resulting in spectacular pulsar wind nebulae (PWNe; see Kargaltsev & Pavlov 2008 for a review) of which the Crab is the most famous example (Weisskopf et al. 2000). The PWN X-ray emission is due to synchrotron radiation from the shocked relativistic outflow of electrons and positrons produced by the pulsar. Magnetars are also expected to produce particle outflows, either steady or released during outbursts accompanying bright bursts or GFs (Thompson & Blaes 1998; Harding et al. 1999; Tong et al. 2012). The GF of 2004 December 27 from SGR J1806−20 released at least 4×10^{43} erg of energy in the form of magnetic fields and relativistic particles (Gaensler et al. 2005). Given the strong magnetic fields associated with this class of neutron stars, the idea, therefore, of a magnetar wind nebula (MWN) seems very plausible.

Only a few claims have been made so far for the detection of a nebula around a magnetar. The first one was the radio nebula around SGR J1806−20 (Kulkarni et al. 1994), which was shown later to be enshrouding a luminous blue variable star, unrelated to the SGR (Hurley et al. 1999). Elongated and expanding radio emission was unambiguously identified following the GF of SGR J1806−20 (Gaensler et al. 2005; Gelfand et al. 2005), most likely associated with jets produced by the flare. A variable radio source indicating particle outflow was also seen after the GF of SGR 1900+14 (Frail et al. 1999). Recently, Rea et al. (2009b), Safi-Harb & Kumar (2008; see also Gonzalez & Safi-Harb 2003), and Vink & Bamba (2009) reported the discovery of unusual extended emission around three high B-field sources, a rotating radio transient, RRAT J1819−1458, a high-B pulsar PSR J1119−6127, and a magnetar 1E 1547.0−5408 (SGR J1550−5418), respectively. The latter case was shown to be a halo on the basis of correlated flux variations in the extended emission and the magnetar (Olausen et al. 2011). In summary, to date there is no unambiguous evidence for the existence of a PWN/MWN around a magnetar. Confirmed detections of MWNe would reconcile observations

with theoretical predictions of their existence and would shed light on the nature of magnetar outflows and the environmental properties of magnetars.

Swift J1834.9−0846 is the last in a long line of magnetar discoveries during the last three years, owing to the synergy between NASA's three observatories, *Swift*, *RXTE*, and *Fermi*. It was discovered on 2011 August 7, when it triggered the *Swift*/Burst Alert Telescope and the *Fermi*/Gamma-ray Burst Monitor with a soft, short burst (D'Elia et al. 2011; Guiriec et al. 2011). The magnetar nature of Swift J1834.9−0846 was established with *RXTE*/PCA and *Chandra* target of opportunity (TOO) observations, which revealed a coherent X-ray pulsation at a spin period $P = 2.482295$ s (Göğüş & Kouveliotou 2011; Göğüş et al. 2011b), and a spin-down rate $\dot{\nu} = -1.3(2) \times 10^{-12}$ Hz s^{-1} (Kuiper & Hermsen 2011), implying a dipole surface magnetic field $B = 1.4 \times 10^{14}$ G, and a spin-down age and energy loss rate $\tau = 4.9$ kyr and $\dot{E}_{\rm rot} = 2.1 \times 10^{34}$ erg s^{-1}, respectively.

Kargaltsev et al. (2012, K+12 hereinafter) studied the spatial, temporal, and spectral properties of Swift J1834.9−0846 using the available *Swift*, *RXTE*, and *Chandra* post-outburst observations, and one *Chandra* pre-outburst observation taken in 2009 June. The persistent X-ray light curve of the source, spanning 48 days after the first burst, showed that the 2–10 keV flux decayed steadily as a power law (PL) with index $\alpha = 0.53 \pm 0.07$ ($F \propto t^{-\alpha}$). The source spectrum (2–10 keV) was well fit with either an absorbed PL with a photon index $\Gamma \approx 3.5 \pm 0.5$ or an absorbed blackbody (BB) with a temperature $kT = 1.1 \pm 0.1$ keV, and an emitting area radius of 0.26 km (assuming a source distance of 4 kpc, see below). The hydrogen column density was of the order of 10^{23} cm^{-2}, depending on the model spectrum. Finally, K+12 reported the presence of an extended emission up to a radius of 10′ from the center of the source, most likely a dust scattering halo, considering the large absorption toward the source position. However, an even more extended emission, with radius >30′, was detected in the 2009 pre-outburst *Chandra* observation. The asymmetrical shape of this emission, northeast–southwest of the source, poses a challenge to the dust scattering halo interpretation, especially since this extended component was detected while the point source was not seen down to a limit of 10^{-15} erg cm^{-2} s^{-1}.

Here, we report the analysis of two *XMM-Newton* observations of Swift J1834.9−0846, taken in 2005 September and 2011 September (one month after the source outburst), with emphasis on the analysis of the environment around the source. Section 2 describes the observations and data reduction techniques. We present our results of the spatial, timing, and spectral analysis in Section 3. We discuss the spectral and temporal results of Swift J1834.9−0846 and the implication of our extended emission analysis in the context of MWN in Section 4. Given a plausible association between Swift J1834.9−0846 and the SNR W41, we will assume that both are at the same distance (∼4 kpc; Tian et al. 2007; Leahy & Tian 2008; K+12) throughout the paper.

2. *XMM-NEWTON* OBSERVATIONS AND DATA REDUCTION

The field of the newly discovered magnetar, Swift J1834.9−0846, was observed twice with *XMM-Newton*. The first observation (ObsID 0302560301, obs. 1 hereafter; PI: Gerd Puehlhofer), taken in 2005 September for an exposure time of about 20 ks, was intended to image the HESS J1834−087 field in which Swift J1834.9−0846 lies. During this observation, Swift J1834.9−0846 was ∼2′ off-axis from the nominal on-axis position, which is small enough not to cause substantial vignetting. The EPIC-PN and MOS detectors were operating in Prime Full Frame mode using the medium filter. Data from all three EPIC instruments were analyzed in the past (EPIC-PN, Tian et al. 2007; EPIC-MOS, Mukherjee et al. 2009). We re-analyzed this observation to look for an extended emission at the position of Swift J1834.9−0846.

The second *XMM-Newton* observation (ObsID 0679380201, obs. 2 hereafter) was a TOO (PI: Norbert Schartel) taken on 2011 September 17 for an exposure of about 24 ks, with Swift J1834.9−0846 being at the aim point of the three EPIC detectors. The EPIC-PN detector was operating in Prime Full Frame mode using the medium filter. The EPIC-MOS detectors, on the other hand, were operating in Small Window mode.

The two observations were reduced and analyzed in a homogeneous manner using the Science Analysis System (SAS) version 11.0.0 and FTOOLS version 6.11.1. Data were selected using event patterns 0–4 and 0–12 for PN and MOS, respectively, during only good X-ray events ("FLAG==0"). We excluded intervals of enhanced particle background during obs. 1, resulting in an effective exposure time of ∼14 ks in the MOS cameras. Response matrices were generated using the task *rmfgen*. These responses were spatially averaged using a point-spread function (PSF) model for point-like sources and a flat uniform flux distribution for extended sources.

Background events for point-like sources were extracted from a source-free region with the same size as the source on the same CCD. We followed the same procedure for the background extraction of extended sources since they only cover a small region in the sky with a size of 2′–3′ (see Section 3.1).

For point-like sources, the background spectrum was directly subtracted from the source spectrum. Such a method corrects for both the instrumental and the cosmic X-ray background simultaneously. Since our extended sources are not very large (see Section 3.1) one can expect that same method would work reasonably well for their spectra. However, to ensure that the background contribution is accurately accounted for, we also tried a more rigorous background-estimate procedure, where we first modeled the background spectrum and then included the background contribution as an additional model component while fitting the source spectrum.

We used the Extended Science Analysis Software (ESAS) package[9] for the purpose of background modeling. First, the instrumental background is extracted from the CCDs where our extended emission lies, using the filter-wheel closed data, i.e., derived from observations where the filter wheel is in the closed position. We correct both the background and the source spectra for the instrumental background. Then, we fit the resulting background spectrum with a combination of two thermal components and an absorbed PL. We froze the temperature of one of the thermal components to 0.1 keV assuming emission from the local hot bubble. The temperature of the second thermal model, which represents the emission from the interstellar/intergalactic medium, was left free to vary (Snowden et al. 2004, 2008). The absorption in the PL was frozen to the Galactic value toward Swift J1834.9−0846, $N_{\rm H} = 1.63 \times 10^{22}$ cm^{-2}, and the photon index of the PL was frozen to 1.5 assuming unresolved active galactic nucleus (AGN) contribution (e.g., distant quasars and/or nearby low-luminosity AGN; Porquet et al. 2004; Sazonov et al. 2008; Younes et al. 2011). We also added a Gaussian emission line with a centroid energy of 1.5 keV to model the instrumental

[9] http://xmm.esac.esa.int/sas/current/doc/esas/index.html

Table 1
Spectral Model Parameters, Fluxes, and Luminosities of Swift J1834.9−0846 and its Surrounding Medium

Source	Model	$N_{\rm H}$ (10^{22} cm^{-2})	Γ	kT (keV)	$N^{\rm a}$ or $R^{\rm b}$	χ^2_ν/dof	$F_{2-10\,\rm keV}$ Absorbed (10^{-12} erg cm^{-2} s^{-1})	$L^{\rm c}_{2-10\rm keV}$ (10^{34} erg s^{-1})
Swift J1834.9−0846 (post-outburst)	PL	24 ± 1	4.2 ± 0.1	...	$5.67^{+0.02}_{-0.01}$	1.15/232	$1.25^{+0.02}_{-0.03}$	$1.6^{+0.2}_{-0.1}$
Swift J1834.9−0846 (post-outburst)	BB	12.9 ± 0.6	...	0.96 ± 0.02	0.24 ± 0.02	1.04/232	$1.19^{+0.03}_{-0.04}$	0.16 ± 0.01
Swift J1834.9−0846 (pre-outburst)[d]	PL	24(fixed)	4.2(fixed)	...	...	...	0.04	0.07
Region A (post-outburst)	PL	25^{+6}_{-5}	$4.5^{+0.7}_{-0.6}$	...	1.48 ± 0.02	0.9/57	0.19 ± 0.02	$0.3^{+0.5}_{-0.2}$
Region A (post-outburst)[e]	PL	31^{+10}_{-9}	$5.0^{+1.0}_{-0.9}$	...	$3.20^{+0.02}_{-0.01}$	0.9/57	0.16 ± 0.02	$0.4^{+0.5}_{-0.2}$
Region A (pre-outburst)	PL	13^{+8}_{-6}	$1.7^{+1.4}_{-1.1}$	...	$0.005^{+0.007}_{-0.003}$	1.3/8	$0.12^{+0.06}_{-0.05}$	$0.04^{+0.02}_{-0.01}$
Region B (post-outburst)	PL	15 ± 5	$3.4^{+1.0}_{-0.9}$	...	0.3 ± 0.1	1.0/23	0.35 ± 0.06	$0.21^{+0.15}_{-0.06}$
Region B (post-outburst)[f]	PL	17 ± 4	$3.2^{+0.7}_{-0.6}$	...	0.2 ± 0.1	0.9/46	0.35 ± 0.04	$0.21^{+0.10}_{-0.06}$
Region B (pre-outburst)	PL	16(fixed)	3.5 ± 0.6	...	$0.2^{+0.2}_{-0.1}$	1.7/19	$0.15^{+0.06}_{-0.05}$	$0.10^{+0.04}_{-0.03}$

Notes.
[a] PL normalization in units of 10^{-2} photons cm^{-2} s^{-1} keV^{-1} at 1 keV.
[b] BB radius, in units of km.
[c] 2–10 keV power-law luminosity or bolometric BB luminosity ($\pi R^2 \sigma T^4$), assuming a source distance of 4 kpc (Tian et al. 2007).
[d] Fluxes and luminosities converted from the count rate in Section 3.1 using *PIMMS*, assuming the corresponding spectral parameters.
[e] Spectral results including the possible contribution from region B (see Section 3.3).
[f] Spectral parameters derived using a modeled background as described in Section 2.

EPIC-PN Al Kα line. The model fit to the background spectrum was good, with $\chi^2_\nu = 1.3$ for 42 degrees of freedom (dof). The temperature of the thermal component is $kT \approx 1.0$ keV, a reasonable value for the intergalactic medium X-ray emission. Finally, we fit the extended emission spectra with an absorbed PL, including the background best-fit model.

The best-fit parameters to our extended sources spectra using the two background-estimation methods, i.e., directly or through modeling, were in very good agreement within the error bars at the 1σ level (Table 1). Hence, in the following the background for extended sources was estimated directly, as usually done for point-like sources.

3. RESULTS

3.1. Spatial Analysis

The X-ray images (1.5–8 keV) of Swift J1834.9−0846 are shown in Figure 1 for obs. 1 (MOS1+2 cameras, lower panel) and obs. 2 (PN camera, upper and middle panels).[10] The middle and lower panels are smoothed with a Gaussian of FWHM $\simeq 20''$ to accentuate the extended emission.

We extracted the radial profile from a set of circular annuli centered at the position of Swift J1834.9−0846 using the MOS1+2 and PN cameras for obs. 1 and obs. 2, respectively (Figure 2). These radial profiles were then fit by re-normalizing an *XMM-Newton* PSF template (to have similar number of counts at the core) and adding a constant background (dot-dashed line). This PSF template, given as an *XMM-Newton* calibration file (XRT3_XPSF_0013.CCF), is the best-fit King function (King 1966) to the radial profile of many bright point sources observed with the EPIC cameras. The rms values of the PSF fit to our radial profiles are 0.10 and 0.35 for obs. 1 and obs. 2, respectively, indicating that a PSF alone is not sufficient to explain the observed source radial profiles, and that an excess emission is present. Indeed, extended emission is clearly visible in both observations, starting at around $15''$ and $25''$ for obs. 1 and obs. 2, respectively. The extent of this emission is larger and more obvious in obs. 2, stretching out to $r \gtrsim 150''$. The emission in obs. 1 is detected up to $r \approx 70''$.

It is clear from Figure 1 (middle panel) that the extended emission around Swift J1834.9−0846 becomes asymmetrical in shape at $r \approx 50''$. We quantified the asymmetrical shape of this extended emission in obs. 2 (which has better statistics than obs. 1), by collapsing the counts in the X (east–west) and Y (south–north) directions, in a rectangular region of 222×91 pixels around the SGR, excluding any point sources in the field. Since our source lies very close to the PN CCD gap, we used an exposure-map-corrected image for this analysis to correct for these CCD gaps, which also corrects for bad pixels. The background level, shown as a black solid line in Figure 3, is the mean value of the total counts in two regions taken at rectangular areas away from the source in both directions. The profile is centered at the SGR central pixel, with the dotted lines representing the $25''$ point-like source emission, i.e., the SGR, and the dashed lines showing the extent of the extended emission. It is clear from both panels of Figure 3 that the extended emission is asymmetrical. In the X-direction, the emission extends up to $\sim 165''$ to the right of the source, but only $\sim 90''$ to the left. In the Y-direction, the emission extends up to $125''$ below the source center and only up to $\sim 45''$ above it.

Finally, we detect in obs. 1 a weak excess emission consistent with a point source at the position of Swift J1834.9−0846. Since the emission around Swift J1834.9−0846 shows an excess over the PSF fit starting at $18''$ (see Figure 2), we estimate the count rate in a $18''$ radius circle centered on the source. We find a rate of 0.0028 ± 0.0006 counts s^{-1}, which represents a detection at the 4.6σ level. We also detect asymmetrical emission west–southwest of the SGR, consistent with the shape and direction of the post-outburst asymmetrical emission discussed above.

We summarize our spatial analysis results in Figure 1. In the post-outburst observation (upper and middle panels), the smallest green circle with a $25''$ radius represents the Swift J1834.9−0846 point-source emission (taking into account the PSF). The green annulus with inner and outer radii of $25''$ and $50''$, respectively (region A hereinafter), represents the

[10] During obs. 1 Swift J1834.9−0846 lies on a CCD gap in the PN camera and these data were not used; obs. 2 used MOS cameras in Small Window mode.

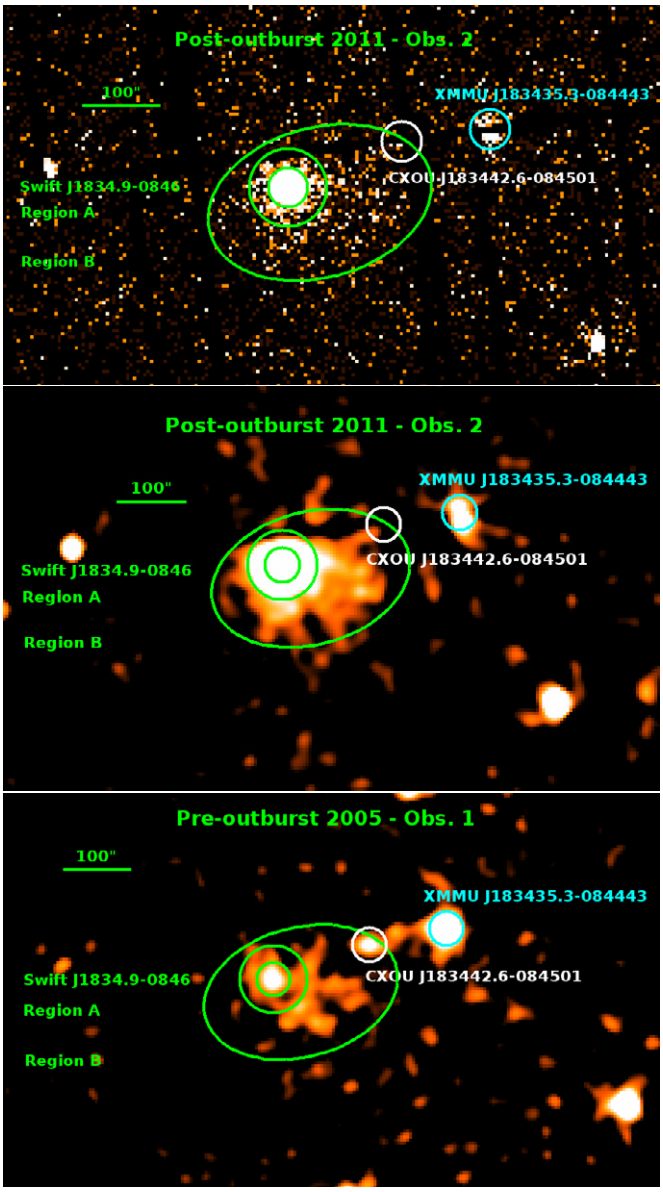

Figure 1. Post-outburst *XMM-Newton* EPIC-PN observation of Swift J1834.9−0846 in 2011 (obs. 2, upper and middle panels) and pre-outburst 2005 EPIC MOS1+MOS2 observation (obs. 1, bottom panel). The middle and bottom images are Gaussian smoothed with an FWHM of 5.0 pixels (20″). The smallest green circle with a 25″ radius represents the Swift J1834.9−0846 point-source emission. The annulus with $25'' \leqslant r \leqslant 50''$ represents the symmetrical extended emission around the point source (region A). The ellipse of major (minor) axis of 145″ (95″) encloses the asymmetrical extended emission around Swift J1834.9−0846 (region B). Other sources in the field are labeled. North is up and west is right.

symmetrical extended emission, most likely a dust scattering halo (see Section 3.3), similar to the one seen in the *Chandra* post-outburst observation (K+12). Beyond $r \sim 50''$ from the center of Swift J1834.9−0846, the asymmetrical extended emission is mostly seen toward the west–southwest of the SGR (middle panel); we approximate this region with an ellipse of major (minor) axis of 145″ (95″) (region B hereinafter). Similar asymmetrical emission is seen in the pre-outburst *XMM-Newton* observation with some hints of weak excess emission at the position of the SGR (lower panel). A similar extended emission has been reported for the *Chandra* pre-outburst observations, when the source was in quiescence (K+12). The asymmetrical shape argues against a dust scattering halo origin, and its small size with the lack of any radio counterpart makes a supernova remnant (SNR) explanation questionable. A third option is, therefore, a wind nebula powered by the magnetar. We will discuss these possibilities in Section 4.

3.2. Timing Analysis

For our timing analysis, which was only performed for obs. 2, we first converted the arrival times of all 2900 events within the 25″ source photon extraction region to the arrival times at the solar system barycenter. We then employed a Z_1^2 test (Buccheri et al. 1983) to search for pulsed signal from the source. We detect the pulsed signal very clearly (with a Z_1^2 peak of about 750) at a frequency of 0.4028466(5) Hz. Note that the measured pulse frequency of Swift J1834.9−0846 is consistent within uncertainties with the spin ephemeris reported by K+12.

We then investigated the energy and time dependence of the pulse profiles. Figure 4 shows the background subtracted pulse profiles in the 2–5, 5–10, and 2–10 keV, respectively, from top to bottom panels. We find that the pulse fraction shows a hint of energy dependence: it is (57 ± 13)% in the 2–5 keV band and (70 ± 17)% in 5–10 keV. The pulsed fraction in the 2–10 keV band is (60 ± 15)%. This value is marginally lower than the value of 85% ± 10% obtained from the *Chandra* observation (K+12), indicating a decline in pulse fraction in over about one month. We also searched for pulse profile evolution in time by splitting the effective duration of the *XMM-Newton* pointing into three parts and generating the pulse profile in each segment in the 2–10 keV range. We find no significant variation of pulse shape throughout the observation as well as between the *XMM-Newton* and *Chandra* observations.

3.3. Spectral Analysis

3.3.1. Post-outburst Observation

Based on our radial profile analysis of obs. 2, we extracted the spectra of Swift J1834.9−0846 in a circular region with a radius of 25″ from the PN camera and with a radius of 20″ from the MOS1/MOS2 cameras (extended emission started at 20″ from the center of the SGR in the MOS cameras), collecting 2900 and 1020 counts, respectively. Background events were extracted from source-free circles with the same radii as for the source and on the same CCD, resulting in 56 and 32, PN and MOS1/MOS2 background counts, respectively. The spectra were then grouped to have a minimum of 25 counts per bin. Finally, we made sure that the point-source spectrum was not affected by pile-up using the *XMM-Newton* SAS task *epatplot*. Table 1 includes the results of our spectral analysis of the point source and both extended regions (see below).

We fit the point-source (Swift J1834.9−0846) spectrum with an absorbed PL and with an absorbed BB model. The latter gave a better fit, with a reduced χ^2 of 1.04 for 232 dof, corresponding to an improvement of 26 in χ^2 for the same number of dof. From the BB fit, we estimate the emitting area radius to be $R = (0.24 \pm 0.02) d_4$ km, where $d_4 = d/4$ kpc, consistent with the value derived from the *Chandra* data taken ∼1 month earlier. Table 1 gives the PL and BB best-fit parameters, and the absorbed fluxes and luminosities. Figure 5 upper (lower) panel shows the best-fit PL (BB) model and the residuals in terms of sigma. In each panel of Figure 5, the upper (black dots) fits are the EPIC-PN data and the two lower fits (blue diamonds and red stars) are the MOS1 and MOS2 data. We note here that the fluxes and luminosities of Swift J1834.9−0846 are half the values derived

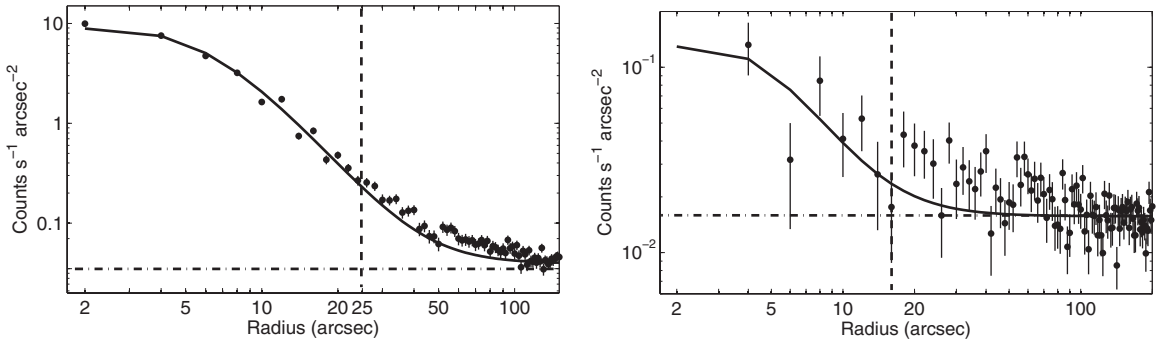

Figure 2. Radial profile of the X-ray emission (1.5–8 keV) of Swift J1834.9−0846 using the *XMM-Newton* data from the post-outburst obs. 2 (PN, left panel) and the pre-outburst obs. 1 (MOS1+2, right panel). The black solid line represents the best-fit PSF for each camera. Extended emission is clearly seen beyond $\sim 20''$ and $\sim 15''$ in obs. 2 and obs. 1, respectively.

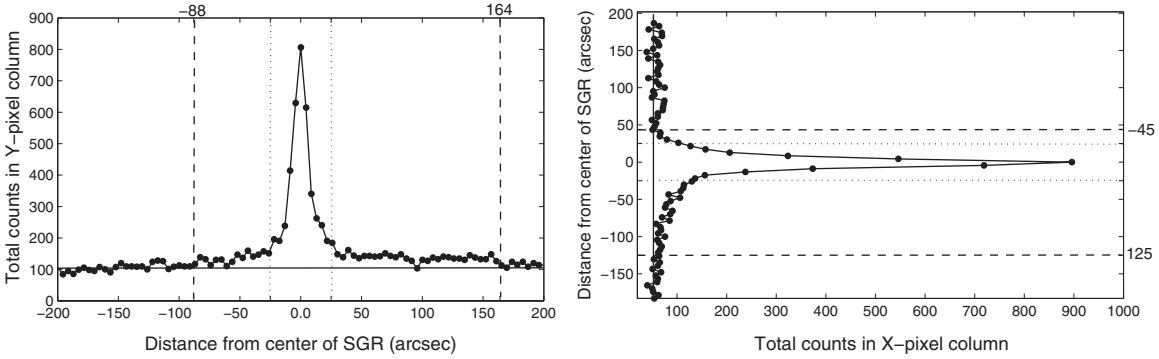

Figure 3. Left column: projected total counts of a pixel column in the *Y*-direction (north–south, left panel) and the *X*-direction (east–west, right panel) in a rectangular region around Swift J1834.9−0846. The dotted lines delimit a $25''$ circular region around the SGR. The dashed lines represent the extent of the asymmetrical extended emission.

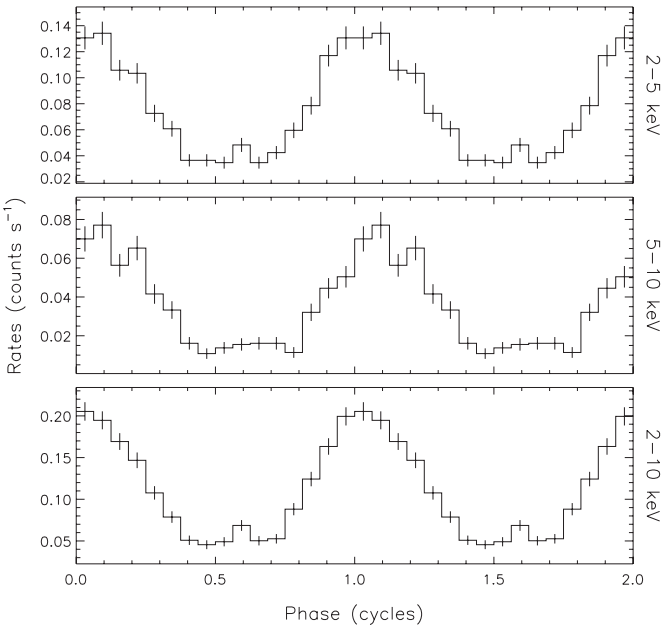

Figure 4. Pulse profiles of the persistent X-ray emission of Swift J1834.9−0846, accumulated between 2–5, 5–10, and 2–10 keV from top to bottom.

from the *Chandra* data almost a month earlier (K+12). Finally, we note that a more complex, two-component model, typically used to fit magnetar X-ray spectra, is not required by the data.

We then binned the spectra of the point source to the PN spectral resolution and searched for potential line-like features in the time-integrated and the time-resolved spectra. The time-integrated spectrum revealed two possible lines (absorption and emission) between 3 and 5 keV. To investigate the lines, we first added a Gaussian emission profile with a best-fit energy of 3.7 keV, which reduced χ^2 by 8, for 3 dof. The addition of an absorption line with a best-fit energy of 4.2 keV resulted in an equal improvement. Adding both lines together does not improve the spectral fit further. We then performed Monte Carlo simulations (MCSs) to rigorously assess the significance of these spectral features. We took the best-fit absorbed PL model as our null hypothesis. We simulated 1000 spectra based on this model with the XSPEC *fakeit* command, and fitted each spectrum with the null hypothesis model. We then added an absorption line to the model (*gabs* in XSPEC) and re-fit the spectrum. For each simulated spectrum, we recorded the $\Delta\chi^2$ between the null hypothesis PL model and the PL + absorption feature model, and compared the values to the real $\Delta\chi^2$. This procedure resulted in an absorption line significance at only the 90% confidence level. Including an emission line at 3.7 keV, instead of an absorption line, gave the same level of significance. We note that this significance level is insensitive to the null hypothesis model since an absorbed BB gave similar results (95% confidence level). We conclude that the lines are not significant in the time-integrated spectrum of Swift J1834.9−0846.

Next, we performed both time-resolved and phase-resolved spectroscopy to investigate whether there are specific intervals (phases) where the lines are more prevalent. For the former case, we split the $\sim$24 ks observation into four equal segments and fit each of the four spectra with an absorbed PL model. We find that the source spectrum is constant throughout the observation. Only in segment two (6.75−13.50 ks) did we see evidence for the presence of an emission line at 3.8 keV (Figure 6, first

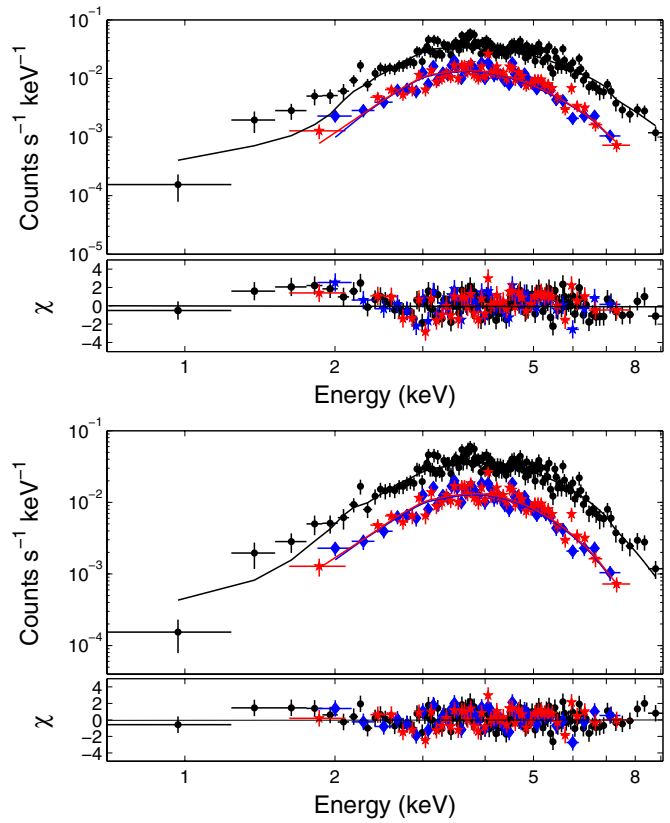

Figure 5. Upper panel: data and power-law fit to the Swift J1834.9−0846 post-outburst *XMM-Newton* data. Lower panel: data and blackbody fit to the Swift J1834.9−0846 post-outburst *XMM-Newton* data. In both panels, black dots, blue diamonds, and red stars represent PN, MOS1, and MOS2 data, respectively. Residuals are shown in terms of sigma.

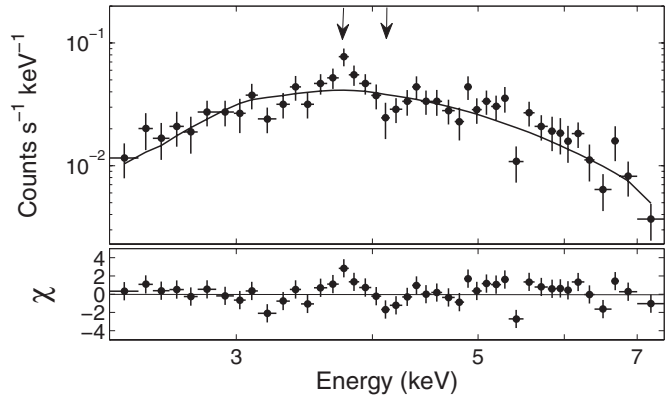

Figure 6. Data and PL fit to the second time segment (see the text) of the post-outburst *XMM-Newton* observation of Swift J1834.9−0846. Residuals are shown in terms of sigma. The arrows indicate potential emission and absorption features at ∼3.7 and 4.2 keV, respectively.

arrow). An MCS showed that the line is significant at the 98.5% confidence level. An MCS of an absorbed BB spectrum with the same emission line resulted in a ∼99% confidence level. The significance is too low to claim a firm line detection; more sensitive observations during a new source burst active episode could provide better statistics.

To perform phase-resolved spectroscopy, we rebinned by a factor of two the profiles of Figure 4, starting at phase = 0, which resulted in a total of eight bins. We then fit each spectrum with an absorbed PL (with $N_{\rm H}$ fixed to the best-fit value, see Table 1). We find no variations across the spectra within uncertainties.

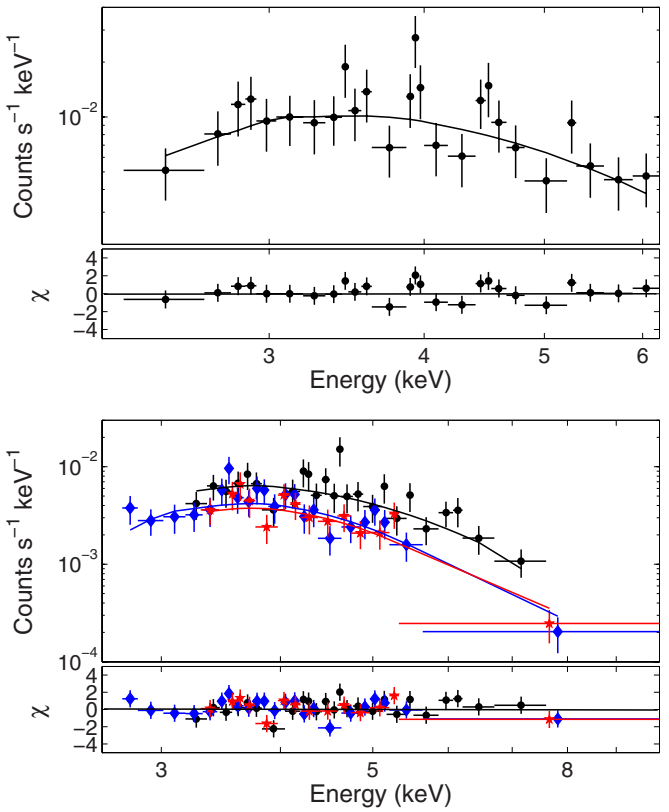

Figure 7. Upper panel: data and power-law fit to region B during the post-outburst *XMM-Newton* observation. Lower panel: data and power-law fit to region A during the post-outburst *XMM-Newton* observation. Black dots, blue diamonds, and red stars represent PN, MOS1, and MOS2 data, respectively. Residuals are shown in terms of sigma.

The high hydrogen column density that we derive for the source suggests that there should be an accompanying dust scattering halo emission (Predehl & Schmitt 1995). Such emission must be symmetrical except for a very unusual dust distribution. Hence, we extracted a spectrum from an annular region $25'' \leqslant r \leqslant 50''$ (region A), from PN, MOS1 and MOS2. The source contribution to the extended emission is supposed to be minimal, including at most 20% from the outer wings of the EPIC-PN PSF.[11] Region A, on the other hand, could contain some contribution from the more extended asymmetrical emission (see Section 3.1). Hence, we modeled the region A spectrum, first, as a separate component, and second taking into account the possible contribution from region B (see below). We find that the spectrum of region A is well fit with an absorbed PL in both cases (Figure 7), with similar $N_{\rm H}$ and photon indices. These parameters are also consistent with those of the SGR within the uncertainties. These results are presented in Table 1 and discussed in Section 4.

We then extracted the PN spectrum of the asymmetrically extended emission (hereafter region B) using an ellipse with a semi-major/minor axis of 145″ and 95″, respectively, which encloses the elliptical region shown in Figure 3. We excluded the Swift J1834.9−0846 and region A extraction areas. The 0.5–10 keV spectrum is adequately fit with an absorbed PL (Figure 6) with a hydrogen column density $N_{\rm H}$ and photon index Γ consistent within uncertainties with those of the point source and region A spectra. Fixing $N_{\rm H}$ to the best-fit value better

[11] http://xmm.esac.esa.int/external/xmm_user_support/documentation/uhb_2.1/

constrains $\Gamma = 3.4^{+0.2}_{-0.3}$; this value is smaller than the point-source index at the 3σ level. All fit parameters and absorbed fluxes and luminosities are given in Table 1.

3.3.2. Pre-outburst Observation

The 2005 *XMM-Newton* observation of the field of Swift J1834.9−0846 shows a weak point-like source at the position of Swift J1834.9−0846. We collected 45 counts from the 18″ radius circle around Swift J1834.9−0846 as shown in the lower panel of Figure 1, not enough for a proper spectral analysis. We, therefore, assumed the same spectral parameters as in the post-outburst observation to derive the 2–10 keV absorbed flux and luminosity listed in Table 1. A photon index $\Gamma = 3.0$, assuming the source X-ray spectrum hardens with declining flux (e.g., Göğüş et al. 2010a), would only decrease the luminosity by a factor of 1.5.

Next, we collected ∼100 counts from region A and binned the spectrum at 15 counts bin^{-1}. We then fit it with an absorbed PL and found that the absorbing column and Γ are consistent, within uncertainties, with the post-outburst values for this region (see also Table 1).

We also extracted the 0.5–10 keV spectrum of region B using the same elliptical region as above (Figure 1), excluding a 50″ radius circle around the Swift J1834.9−0846 position. This resulted in a total of ∼90 counts. Because of the low statistics we grouped the spectrum to have 40 counts per bin, achieving a signal-to-noise ratio (S/N) of ∼2 (this low S/N is due to the large background of MOS1/MOS2 compared with the extended emission photon flux). We fit the spectrum with an absorbed PL. We also fixed the column density to the best-fit value, $N_{\rm H} = 1.6 \times 10^{23}$ cm^{-2}, and found $\Gamma = 3.5 \pm 0.6$, consistent with the post-outburst extended emission value. The absorbed flux and luminosity of region B are roughly a factor of two lower than their post-outburst values. These results are also discussed in Section 4.

4. DISCUSSION

4.1. Swift J1834.9−0846

The effects of bursting activity on the magnetar persistent X-ray flux have been discussed by several authors. The increase of the source intensity during bursting episodes is also often accompanied by spectral variability (e.g., Vasisht et al. 2000; Gotthelf et al. 2004; Göğüş et al. 2010b). It would then be reasonable to assume that the detection of Swift J1834.9−0846 in the 2005 *XMM-Newton* observation at $F_{2-10\,\rm keV} \approx 10^{-13}$ erg cm^{-2} s^{-1}, could be due to a bursting episode that had occurred prior and close to that observation (if such an episode comprised only one burst similar to the 2011 episode, it could have easily been missed by *Swift*, which was the only all sky monitor in the 25–350 keV range at the time). Indeed, assuming a (constant) flux decay trend between 2005 and 2009 similar to the one exhibited by the source after its 2011 outburst ($\alpha = -0.5$, Figure 8) results in an expected flux level in 2009, consistent with the estimated upper limit of 10^{-15} erg cm^{-2} s^{-1} (K+12).

However, there may be other sources of neutron star surface heating that might not result in SGR bursts, such as was the case of the transient magnetar SGR J1810−197 (Ibrahim et al. 2004). The source was serendipitously discovered with *RXTE* as a transient during observations of a nearby magnetar (SGR J1806−20); the increase of its X-ray flux was not associated with any bursting activity during that period. This behavior could be explained within the framework of the twisted magnetosphere model of Thompson et al. (2002) as follows. Variations of the twist angle of the magnetic field lines would lead to a sudden release of energy accompanied by possible changes in the cyclotron resonant scattering depth in the magnetosphere and heating of the neutron star surface. Heating by such a *B*-field reconfiguration should also be associated with sharp spectral changes. Unfortunately, with the currently available data we cannot distinguish between the two scenarios.

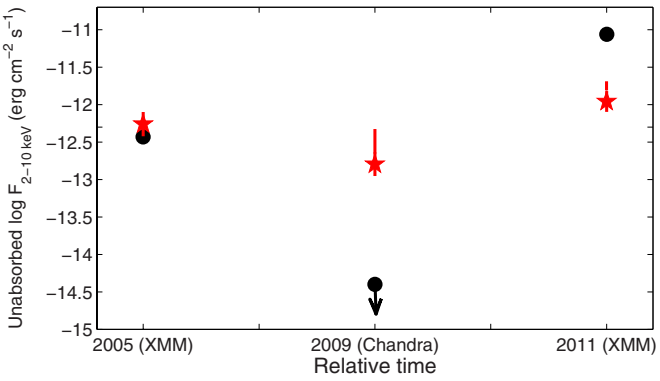

Figure 8. Long-term light curves of the fluxes (2–10 keV) of Swift J1834.9−0846 (black dots) and region B (red stars).

Magnetar X-ray spectra are usually fit by a two-component model, e.g., two BBs with temperatures $kT_1 \sim 0.3$ keV and $kT_2 \sim 0.8$ keV, or a BB and a PL with $kT \sim 0.5$ keV and $\Gamma \sim 3.0$–4.0 (e.g., Mereghetti et al. 2005; Halpern & Gotthelf 2005; Tiengo et al. 2008; Bernardini et al. 2009, 2011; Rea et al. 2009a; Göğüş et al. 2011a; Woods et al. 2007; Kouveliotou et al. 2003, 2001). The 2005 pre-outburst spectral properties of the source could not be inferred due to very low statistics. The post-outburst X-ray spectrum of Swift J1834.9−0846 seems unusual at first glance, as it is well fit by a single, heavily absorbed ($N_{\rm H} \sim 10^{23}$ cm^{-2}) component, either a BB with $kT = 1.1$ keV or a PL with $\Gamma = 4.2$ (see also K+12). It could be that we see here the effects of the environment within which Swift J1834.9−0846 resides; e.g., dense giant molecular clouds (GMCs; Tian et al. 2007), which, in principle, could absorb the soft part of the spectrum, eliminating the requirement of a soft spectral component (see also Esposito et al. 2011).

The single BB spectral model for Swift J1834.9−0846 gives a small decrease in the BB temperature ($\Delta kT = 0.14 \pm 0.06$ keV), and a consistent BB emitting area radius ($\Delta R = 0.02 \pm 0.05$) between the *Chandra* and *XMM-Newton* post-outburst observations separated by a month, similar to the behavior of XTE J1810−197 (Woods et al. 2005). The BB fluxes between the two observations are consistent with the same PL decay $\alpha \approx -0.5$, estimated using the PL fits. K+12 discussed the possibility of a hot spot emitting thermal radiation at the surface of the neutron star, noting that in such a scenario it would be difficult to explain the high pulsed fraction due to light bending in the neutron star gravitational field, unless the radiation is anisotropic, having a narrow peak along the magnetic field direction (Pavlov et al. 1994).

4.2. A Halo around Swift J1834.9−0846: Region A

The spectrum and flux of the symmetrical extended emission (region A) fits well a dust scattering halo interpretation. First, the heavy absorption ($N_{\rm H} \approx 10^{23}$ cm^{-2}) toward the source, inferred from the X-ray spectral fits, should cause the scattering of the point-source X-ray emission, resulting in a dust scattering

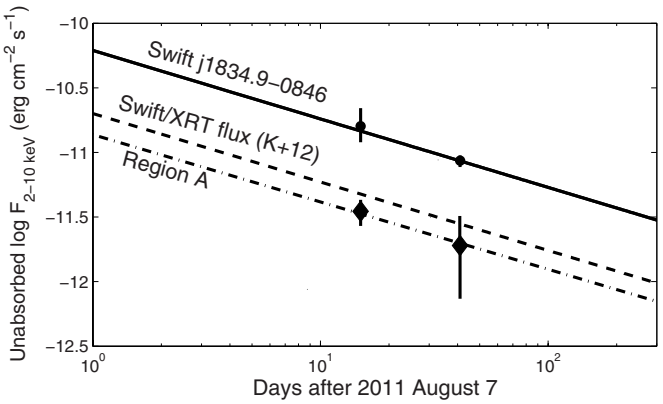

Figure 9. Post-outburst persistent X-ray light curve of Swift J1834.9−0846 based on 48 days of *Swift*/XRT data (dashed line, K+12); day 1 corresponds to the *Swift* trigger. The dots represent the *Chandra* and *XMM-Newton* post-outburst point-source fluxes (2–10 keV), respectively, while the diamonds represent the fluxes of region A during the same observations. The dashed line represents the *Swift*/XRT decay slope of −0.5; the solid and dot-dashed lines are decay trends of the point source and region A with the same slope.

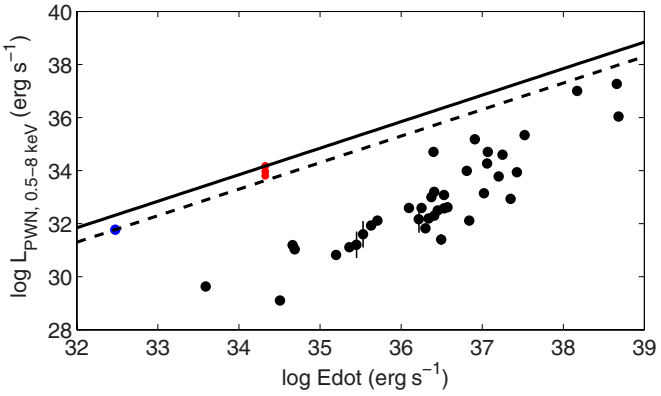

Figure 10. Luminosity of normal PWNe as a function of the rotational energy loss of their corresponding pulsars. Data presented as black dots are taken from Kargaltsev & Pavlov (2008), whereas the blue star represents the high-*B* source RRAT J1819−1458 (Rea et al. 2009b). The dashed line represents the $\eta_X = 0.2$ of RRAT J1819−1458, and the solid line represents the $\eta_X = 0.7$ of Swift J1834.9−0846. The three red dots represent the luminosity of the candidate MWN around Swift J1834.9−0846 at the detected epochs. (Figure adapted from Rea et al. 2009b.)

halo. Since the scattering cross section of the dust particles is proportional to E^{-2}, a halo is expected to have a softer spectrum than the illuminating source, i.e., Swift J1834.9−0846. Indeed, in obs. 2, the spectrum of region A is marginally softer than the Swift J1834.9−0846 spectrum (although consistent within the uncertainties, see Section 3.3 and Table 1). Second, a dust scattering halo is expected to vary in flux proportionally to the illuminating source flux (Mathis & Lee 1991), with a time lag depending on the distance of the scattering material from the source (Mauche & Gorenstein 1986; Olausen et al. 2011). This trend is evident from Figure 9, which shows the flux evolution of region A and Swift J1834.9−0846, between the post-outburst *Chandra* (K+12) and *XMM-Newton* observations (diamonds). Finally, we estimate the fractional intensity of the halo during obs. 2 to be $I_{\rm frac} = F_{\rm halo}/(F_{\rm halo} + F_{\rm source}) = 0.20^{+0.25}_{-0.10}$.

During obs. 1 the spectrum of region A was harder, $\Gamma = 1.7^{+1.4}_{-1.1}$, with a fractional intensity $I_{\rm frac} = 0.36^{+0.2}_{-0.1}$, somewhat higher than, but consistent within the error bars with the $I_{\rm frac}$ calculated for obs. 2. However, the Swift J1834.9−0846 spectrum during obs. 1 is unknown due to the poor statistics. The harder spectrum during obs. 1 could then be explained if there was another component contributing to the flux in region A. Indeed, the flux of region B (the putative MWN, see Section 4.3) dominates the emission from the vicinity of Swift J1834.9−0846 during obs. 1 (Table 1), which could explain both the hard spectrum and the slightly higher $I_{\rm frac}$ seen during this observation. Another explanation could be that the Swift J1834.9−0846 spectrum during obs. 1 is much harder than it is during obs. 2, which would make the region A spectral shape consistent with a solely dust scattering halo explanation.

4.3. Asymmetrical Extended Emission (Region B): An MWN?

RPPs with magnetic fields $B \sim 10^{11-13}$ G and periods $P \lesssim 1$ s are believed to lose their rotational energy in the form of a relativistic magnetized particle wind. PWNe are often observed around these pulsars and are believed to be the synchrotron radiation of the shocked wind (see Kaspi et al. 2006; Gaensler & Slane 2006; Kargaltsev & Pavlov 2008, for reviews). The efficiency at which the rotational energy loss of a pulsar, $\dot{E}_{\rm rot}$, is radiated by the PWN is characterized by $\eta_X = L_{\rm X,PWN}/\dot{E}_{\rm rot}$, which ranges from 10^{-6} to 10^{-2}. Magnetars, on the other hand, have longer spin periods and lower $\dot{E}_{\rm rot}$ values, making the production of a steady and bright rotationally powered nebula unlikely. Nonetheless, Thompson & Blaes (1998) showed that particle outflows, either steady or released in short periods of time due to the flares, could be driven by Alfvén waves (see also Harding et al. 1999). Furthermore, a jetted baryonic outflow was observed in the radio wavelengths after the GF of SGR J1806−20 (Gaensler et al. 2005; Fender et al. 2006). These processes could lead to the emergence of nebulae around magnetars.

There has not been yet a ubiquitous detection of an MWN in X-rays, but "magnetically powered" nebulae around pulsars with relatively high magnetic fields have been suggested. Rea et al. (2009b) reported that the nebula around the rotating radio transient RRAT J1819−1458 has a nominal X-ray efficiency $\eta_X \approx 0.2$, too high to be rotationally powered. The authors suggested that the occurrence of the nebula might be connected with the high magnetic field ($B = 5 \times 10^{13}$ G) of the pulsar.

The nebula around Swift J1834.9−0846 shares some characteristics with the nebula around RRAT J1819−1458. The X-ray efficiency of the Swift J1834.9−0846 nebula is very high, $\eta_X \approx 0.7$, for a 0.5–8 keV luminosity of 1.5×10^{34} erg s^{-1}.[12] Considering the source's relatively low rotational energy loss ($\dot{E}_{\rm rot} = 2.1 \times 10^{34}$ erg s^{-1}), it is in the low-$\dot{E}_{\rm rot}$/high-$L_{\rm X,PWN}$ region in Figure 10, similar to RRAT J1819−1458. Moreover, the nebula around Swift J1834.9−0846 shows small flux variability (owing to large uncertainties) between the three different epochs (Figure 9). Its flux slightly decreased, although within uncertainties, when the source went to quiescence in 2009 ($F_X < 10^{-15}$ erg s^{-1}), then increased by a factor of seven (at the $\sim 2\sigma$ level) after the 2011 September outburst, in line with a variable wind nebula scenario.

An obvious difference between the MWN around Swift J1834.9−0846 and the "usual" PWNe is the very soft spectrum of the former, $\Gamma = 3.5 \pm 0.6$, compared with $\Gamma \sim 1$–2 of PWNe of RPPs. It is worth pointing out that the nebula around RRAT J1819−1458 also shows a soft spectrum, $\Gamma = 3.0 \pm 0.5$, which suggests that the two nebulae are in some respects similar; in

[12] We have chosen the 0.5–8 keV energy range to enable comparison with the efficiency of RRAT J1819−1458 and other pulsars; see Figure 10.

particular, the electrons are accelerated by similar mechanisms (we note, however, that the nebula around RRAT J1819−1458 is about 10 times smaller in size than the nebula around Swift J1834.9−0846, for similar distances). For the most plausible assumption that we are observing synchrotron radiation of relativistic electrons, this large index implies a very steep electron spectrum, with a slope $p = 2\Gamma - 1 \approx 6$. What could produce such an electron population? A different mechanism (other than the typically invoked Fermi mechanism) of electron acceleration, such as, e.g., magnetic field line reconnection might be at work. We can only conjecture that the twisted magnetic field model by Thompson et al. (2002) could lead to reconnection, facilitating the production of the required electron population distribution.

We can estimate the termination shock radius R_s depending on our assumptions about the energy flux provided by the magnetar. In quiescence, the balance of pressures $\dot{E}_{\rm rot}/(4\pi f c R_s^2) = p$, where $4\pi f$ is the solid angle in which the wind (including the Poynting flux) is blowing ($f = 1$ for an isotropic wind), and p is the ambient pressure (this equation assumes that the magnetar's speed is essentially subsonic). For the $\dot{E}_{\rm rot} = 2.1 \times 10^{34}$ erg s^{-1}, this equation gives $R_s = 2.4 \times 10^{16} f^{-1/2} p_{-10}^{-1/2}$ cm, where p_{-10} is the pressure in units of 10^{-10} erg cm^{-3}. This corresponds to the angular size of $0\farcs4 f^{-1/2} p_{-10}^{-1/2} d_4^{-1}$. Such a small size cannot be resolved by *XMM-Newton*, and it is hidden within the dust scattering halo (region A), assuming reasonable values for the ambient pressure. The size of an X-ray PWN is typically a factor of a few times larger than R_s (e.g., Kargaltsev & Pavlov 2008), which is still much smaller than the observed size of $\sim$150″. Therefore, not only the unrealistically high "efficiency" $\eta_{\rm X} \sim 0.7$, but also the large size support the hypothesis that the observed asymmetrical nebula (region B) could not be produced by the magnetar in quiescence via rotation-powered wind.

When a magnetar is in an active state, the pressure of its wind (ejected particles and magnetic fields) is much higher than that in quiescence. In this state, the energy loss rate, $\dot{E}_{\rm burst}$, can be much higher than $\dot{E}_{\rm rot}$. It can be crudely estimated as a ratio of the magnetar's X-ray luminosity in the bursting state, $L_X = 10^{34} L_{X,34}$ erg s^{-1}, to some reasonable magnetar X-ray efficiency $\eta_{\rm X} = 10^{-4}\eta_{\rm X,-4}$: $\dot{E}_{\rm burst} = 10^{38} L_{X,34}\eta_{\rm X,-4}^{-1}$ erg s^{-1}. Using $\dot{E}_{\rm burst}$ instead of $\dot{E}_{\rm rot}$, we obtain $R_s = 1.6 \times 10^{18} L_{X,34}^{1/2}\eta_{\rm X,-4}^{-1/2} f^{-1/2} p_{-10}^{-1/2}$ cm, which corresponds to the angular shock radius of $\sim 25'' \, L_{X,34}^{1/2}\eta_{\rm X,-4}^{-1/2} f^{-1/2} p_{-10}^{-1/2} d_4^{-1}$, and a factor of a few larger size of the X-ray nebula, comparable with the observed nebula radius of $\sim$150″. This allows one to assume that the detected nebula was created in a burst (or a series of bursts), which is in line with our first assumption in Section 4.1, that likely the magnetar experienced a bursting episode before obs. 1, which was not directly detected.

We can in principle connect the nebula size (and even the softness of the spectrum) with synchrotron cooling. First of all, it is worth noting that the magnetic field at the shock (if there is a shock) does *not* depend on the neutron star surface magnetic field—it is determined by the balance of the wind pressure and the ambient pressure and depends on the latter and the magnetization parameter σ (i.e., the ratio of the electromagnetic energy flux to the kinetic energy flux): $B_s \sim [8\pi\sigma p/(1+\sigma)]^{1/2} \sim 50[p_{-10}\sigma/(1+\sigma)]^{1/2}$ μG, upstream of the shock, and it can be a factor of three higher immediately downstream of the shock (Kennel & Coroniti 1984). This, in particular, means that the softness of the nebula spectrum is not due to a higher magnetic field in the nebula. The magnetization parameter σ is, unfortunately, quite uncertain for the putative magnetar winds. It is believed to be $\ll 1$ for PWNe (e.g., $\sim 10^{-3}$ for the Crab), but it may be higher in magnetars. Therefore, the actual value of the magnetic field in the shocked magnetar flow remains uncertain; it might be as low as a few μG (for small σ and low-pressure ambient medium) or as high as a few mG (for large σ and high-pressure medium). Therefore, we will simply scale the field as $B = 10^{-4} B_{-4}$ G.

The synchrotron cooling time for an electron with Lorentz factor γ can be estimated as $\tau_{\rm syn} = 5 \times 10^8 \gamma^{-1} B^{-2}$ s $\sim 5 \times 10^8 \gamma_8^{-1} B_{-4}^{-2}$ s $\sim 5 \times 10^8 B_{-4}^{-3/2}$ s, where for synchrotron emission in the X-ray band we used $\gamma_8^2 B_{-4} \sim (E/5\,{\rm keV})$.

The shocked wind flows from the magnetar with mildly relativistic velocities (e.g., $c/3$ for an isotropic outflow—see Kennel & Coroniti 1984). Multiplying $\tau_{\rm syn}$ by the flow velocity, we obtain a distance from the magnetar where the X-ray synchrotron radiation still can be observed: $R_{\rm MWN} \sim 5 \times 10^{18} B_{-4}^{-3/2}$ cm, which corresponds to an angular distance of $\sim 84'' \, B_{-4}^{-3/2}$, quite close to the observed size for $B \sim 60$ μG. Thus, the observed size can be explained by the synchrotron cooling of the outflowing electrons in a reasonable magnetic field.

The cooling time also determines the lifetime of the putative MWN after the end of the magnetar activity period. For instance, for $B \sim 60$ μG, $\tau_{\rm syn} \sim 30$ years, which means that the MWN can be observable in X-rays around quiescent (even undetectable) magnetars if these were in an active state years ago; it would also explain the detection of the MWN in obs. 1.

Finally, we would like to discuss some other possibilities for the origin of the extended X-ray emission around Swift J1834.9−0846. The source lies in the center of a crowded field filled with many other high energy sources. It lies almost at the center of the extended TeV source HESS J1834−087 (Aharonian et al. 2006), and within the SNR W41 (K+12) and a dense GMC (Tian et al. 2007). The high absorbing column density toward Swift J1834.9−0846 is most likely related to the GMC, which in turn is causing the scattering halo emission. An anisotropic dust distribution within the GMC could cause an asymmetrical halo emission, leading to region A and region B emanating from the same region and having the same physical origin. To test this hypothesis, we extracted the spectrum of region A+region B during obs. 2 and fit it with an absorbed PL. We find a hydrogen column density $N_{\rm H} = 17^{+4}_{-3} \times 10^{22}$ cm^{-2}, consistent with the point-source absorbing column, and a PL photon index $\Gamma = 3.4 \pm 0.5$, harder than the point-source spectrum, indicating that a halo interpretation for region A+region B is unlikely. Hence, the nature of these two regions is indeed different, as indicated by their different spectral properties (Section 3.3). Moreover, the detection of region B during obs. 1, when the source was in quiescence, poses a challenge to such an interpretation. Another possibility for the region B emission could be some contribution from the SNR W41, in the form of either thermal emission from shocked gas or non-thermal synchrotron emission (see Vink 2012, for a review). However, the fluxes of both region A and region B varied with the source flux, implying a tight connection between the two and the SGR. Deeper high-resolution multiwavelength observations would be of great value to better understand the physical properties and emission processes of the Swift J1834.9−0846 putative MWN, and would help shed light on the connections between the many point-like and extended sources existing in this crowded field.

This work is based on observations with *XMM-Newton* an ESA science mission with instruments and contributions directly funded by ESA Member States and the USA (NASA). The work by O.Y.K. and G.G.P. was partly supported by NASA grants NNX09AC81G and NNX09AC84G, NSF grants AST09-08733 and AST09-08611, and by the Ministry of Education and Science of the Russian Federation (contract 11.G34.31.0001). The authors are grateful to Norbert Schartel for his decision to allocate *XMM-Newton* TOO time for observation of Swift J1834.9−0846. The authors thank the referee for the constructive comments that helped improve the quality of the manuscript.

REFERENCES

Aharonian, F., Akhperjanian, A. G., Bazer-Bachi, A. R., et al. 2006, ApJ, 636, 777
Bernardini, F., Israel, G. L., Dall'Osso, S., et al. 2009, A&A, 498, 195
Bernardini, F., Israel, G. L., Stella, L., et al. 2011, A&A, 529, A19
Buccheri, R., Bennett, K., Bignami, G. F., et al. 1983, A&A, 128, 245
D'Elia, V., Barthelmy, S. D., Baumgartner, W. H., et al. 2011, GRB Coordinates Network, 12253, 1
Duncan, R. C., & Thompson, C. 1992, ApJ, 392, L9
Esposito, P., Israel, G. L., Turolla, R., et al. 2011, MNRAS, 416, 205
Fender, R. P., Muxlow, T. W. B., Garrett, M. A., et al. 2006, MNRAS, 367, L6
Frail, D. A., Kulkarni, S. R., & Bloom, J. S. 1999, Nature, 398, 127
Gaensler, B. M., Kouveliotou, C., Gelfand, J. D., et al. 2005, Nature, 434, 1104
Gaensler, B. M., & Slane, P. O. 2006, ARA&A, 44, 17
Gelfand, J. D., Lyubarsky, Y. E., Eichler, D., et al. 2005, ApJ, 634, L89
Göğüş, E., Cusumano, G., Levan, A. J., et al. 2010a, ApJ, 718, 331
Göğüş, E., Güver, T., Özel, F., Eichler, D., & Kouveliotou, C. 2011a, ApJ, 728, 160
Göğüş, E., & Kouveliotou, C. 2011, ATel, 3542, 1
Göğüş, E., Kouveliotou, C., Kargaltsev, O., & Pavlov, G. 2011b, ATel, 3576, 1
Göğüş, E., Woods, P. M., Kouveliotou, C., et al. 2010b, ApJ, 722, 899
Gonzalez, M., & Safi-Harb, S. 2003, ApJ, 591, L143
Gotthelf, E. V., Halpern, J. P., Buxton, M., & Bailyn, C. 2004, ApJ, 605, 368
Guiriec, S., Kouveliotou, C., & van der Horst, A. J. 2011, GRB Coordinates Network, 12255, 1
Halpern, J. P., & Gotthelf, E. V. 2005, ApJ, 618, 874
Harding, A. K., Contopoulos, I., & Kazanas, D. 1999, ApJ, 525, L125
Hurley, K., Kouveliotou, C., Cline, T., et al. 1999, ApJ, 523, L37
Ibrahim, A. I., Markwardt, C. B., Swank, J. H., et al. 2004, ApJ, 609, L21
Kargaltsev, O., Kouveliotou, C., Pavlov, G. G., et al. 2012, ApJ, 748, 26
Kargaltsev, O., & Pavlov, G. G. 2008, in AIP Conf. Seri. 983, 40 Years of Pulsars: Millisecond Pulsars, Magnetars and More, ed. C. Bassa, Z. Wang, A. Cumming, & V. M. Kaspi (Melville, NY: AIP), 171
Kaspi, V. M., Roberts, M. S. E., & Harding, A. K. 2006, in Isolated Neutron Stars, ed. W. H. G. Lewin & M. van der Klis (Cambridge: Cambridge Univ. Press), 279
Kennel, C. F., & Coroniti, F. V. 1984, ApJ, 283, 710
King, I. R. 1966, AJ, 71, 64
Kouveliotou, C., Dieters, S., Strohmayer, T., et al. 1998, Nature, 393, 235
Kouveliotou, C., Eichler, D., Woods, P. M., et al. 2003, ApJ, 596, L79
Kouveliotou, C., Strohmayer, T., Hurley, K., et al. 1999, ApJ, 510, L115
Kouveliotou, C., Tennant, A., Woods, P. M., et al. 2001, ApJ, 558, L47
Kuiper, L., & Hermsen, W. 2011, ATel, 3577, 1
Kulkarni, S. R., Frail, D. A., Kassim, N. E., Murakami, T., & Vasisht, G. 1994, Nature, 368, 129
Leahy, D. A., & Tian, W. W. 2008, AJ, 135, 167
Mathis, J. S., & Lee, C.-W. 1991, ApJ, 376, 490
Mauche, C. W., & Gorenstein, P. 1986, ApJ, 302, 371
Mereghetti, S. 2008, A&AR, 15, 225
Mereghetti, S., Tiengo, A., Esposito, P., et al. 2005, ApJ, 628, 938
Mukherjee, R., Gotthelf, E. V., & Halpern, J. P. 2009, ApJ, 691, 1707
Olausen, S. A., Kaspi, V. M., Ng, C.-Y., et al. 2011, ApJ, 742, 4
Paczynski, B. 1992, Acta Astron., 42, 145
Pavlov, G. G., Shibanov, Y. A., Ventura, J., & Zavlin, V. E. 1994, A&A, 289, 837
Porquet, D., Reeves, J. N., O'Brien, P., & Brinkmann, W. 2004, A&A, 422, 85
Predehl, P., & Schmitt, J. H. M. M. 1995, A&A, 293, 889
Rea, N., Israel, G. L., Turolla, R., et al. 2009a, MNRAS, 396, 2419
Rea, N., McLaughlin, M. A., Gaensler, B. M., et al. 2009b, ApJ, 703, L41
Safi-Harb, S., & Kumar, H. S. 2008, ApJ, 684, 532
Sazonov, S., Krivonos, R., Revnivtsev, M., Churazov, E., & Sunyaev, R. 2008, A&A, 482, 517
Snowden, S. L., Collier, M. R., & Kuntz, K. D. 2004, ApJ, 610, 1182
Snowden, S. L., Mushotzky, R. F., Kuntz, K. D., & Davis, D. S. 2008, A&A, 478, 615
Thompson, C., & Blaes, O. 1998, Phys. Rev. D, 57, 3219
Thompson, C., & Duncan, R. C. 1995, MNRAS, 275, 255
Thompson, C., & Duncan, R. C. 1996, ApJ, 473, 322
Thompson, C., Lyutikov, M., & Kulkarni, S. R. 2002, ApJ, 574, 332
Tian, W. W., Li, Z., Leahy, D. A., & Wang, Q. D. 2007, ApJ, 657, L25
Tiengo, A., Esposito, P., & Mereghetti, S. 2008, ApJ, 680, L133
Tong, H., Xu, R. X., Song, L. M., & Qiao, G. J. 2012, arXiv:1205.1626
Vasisht, G., Gotthelf, E. V., Torii, K., & Gaensler, B. M. 2000, ApJ, 542, L49
Vink, J. 2012, A&AR, 20, 49
Vink, J., & Bamba, A. 2009, ApJ, 707, L148
Weisskopf, M. C., Hester, J. J., Tennant, A. F., et al. 2000, ApJ, 536, L81
Woods, P. M., Kouveliotou, C., Finger, M. H., et al. 2007, ApJ, 654, 470
Woods, P. M., Kouveliotou, C., Gavriil, F. P., et al. 2005, ApJ, 629, 985
Woods, P. M., & Thompson, C. 2006, in Soft Gamma Repeaters and Anomalous X-ray Pulsars: Magnetar Candidates, ed. W. H. G. Lewin & M. van der Klis (Cambridge: Cambridge Univ. Press), 547
Younes, G., Porquet, D., Sabra, B., & Reeves, J. N. 2011, A&A, 530, A149